

# SENSITIVITY STUDY OF A NUMERICAL MODEL OF HEAT AND MASS TRANSFER INVOLVED DURING THE MEDIUM-DENSITY FIBERBOARD HOT PRESSING PROCESS

*Zanin Kavazovic*<sup>†</sup>

PhD Candidate

*Jean Deteix*

Research Associate

Groupe Interdisciplinaire de Recherche en Éléments Finis  
Département de Mathématiques et de Statistique  
1045, Avenue de la Médecine  
Université Laval  
Québec (QC), Canada, G1V 0A6

*Alain Cloutier*<sup>\*†</sup>

Professor

Centre de Recherche sur le Bois  
Département des Sciences du Bois et de la Forêt  
2425, Rue de la Terrasse  
Université Laval  
Québec (QC), Canada, G1V 0A6

*André Fortin*

Professor

Groupe Interdisciplinaire de Recherche en Éléments Finis  
Département de Mathématiques et de Statistique  
1045, Avenue de la Médecine  
Université Laval  
Québec (QC), Canada, G1V 0A6

(Received July 2009)

**Abstract.** The objective of this work was to estimate the impact of the variability of the medium-density fiberboard mat heat and moisture transfer properties on the results predicted by a numerical model of hot pressing. The three state variables of the model, temperature, air pressure, and vapor pressure, depend on parameters describing the material properties of the mat known with a limited degree of precision. Moreover, different moisture sorption models and initial moisture contents also have an impact on the numerically predicted results. In this sensitivity study, we determined the impact of variations of the mat properties, sorption models, boundary conditions, and initial MC on the state variables. Our study shows that mat thermal conductivity, convective mass transfer coefficient of the external boundary, and gas permeability have the most significant impact on temperature, gas pressure, and MC within the mat. On the other hand, the convective heat transfer coefficient of the external boundary has no impact on the state variables. The sorption model affects significantly mat MC predictions only. The initial MC of the mat has a strong influence on the internal gas pressure.

**Keywords:** Sensitivity study, hot pressing, heat and mass transfer, finite element method, sorption models, initial moisture content, material properties.

## INTRODUCTION

The hot pressing of medium-density fiberboard (MDF) is a complex process involving several heat and mass transfer properties of the fiber

---

\* Corresponding author: [alain.cloutier@sbf.ulaval.ca](mailto:alain.cloutier@sbf.ulaval.ca)

† SWST member

mat. It has captured the attention of many researchers over the last few years. A comprehensive literature review can be found in Bolton and Humphrey (1988). Among the first researchers proposing an integrated approach were Kavvouras (1977), Humphrey (1982), and Humphrey and Bolton (1989a). The first multidimensional heat and moisture transfer model was probably proposed and developed by Humphrey (1982). A series of papers describing the physics involved in the hot pressing of particleboard and presenting typical predictive results followed (Bolton et al 1989a, 1989b, 1989c; Humphrey and Bolton 1989a). That work is the foundation on which the comprehensive model proposed by Thömen and Humphrey (2006) was developed.

Different heat and mass transfer models describing the hot pressing process of wood-based composite panels such as MDF, oriented strandboard, and particleboard have been proposed (Bolton et al 1989a, 1989b; Humphrey and Bolton 1989a; Carvalho and Costa 1998; Zombori et al 2003; Dai and Yu 2004; Nigro and Storti 2006; Thömen and Humphrey 2006). Ultimately, all the heat and mass transfer models are based on the mass conservation of air and water vapor and conservation of heat (Zombori et al 2003; Dai and Yu 2004; Thömen and Humphrey 2006). To these conservation laws, one can add the cure kinetics equation of the adhesive system to predict the evolution of resin cure (Loxton et al 2003; Zombori et al 2003). An appropriate model of moisture sorption is also required (Malmquist 1958; Nelson 1983; Wu 1999; Dai and Yu 2004; Vidal Bastías and Cloutier 2005).

The numerically predicted solutions depend on several heat and mass transfer properties of the fiber mat. Most of these properties are known to a limited degree of precision, especially under conditions prevailing during the hot pressing process. Moreover, most of the material properties are obtained from measurements made on wood or on manufactured panels (von Haas et al 1998). Furthermore, mats made from fibers of different morphology will most likely have different properties. We understand that these specifics have an impact on the precision of the numerical results. To

improve the reliability of a mathematical model as a predictive tool in the development of wood-based composite products, a better understanding of the influence of the material properties on the mathematical model results is needed. Therefore, the model sensitivity to the parameters characterizing heat and mass transfer in the fiber mat must be examined (Zombori et al 2004).

Another important component of every mathematical model of heat and mass transfer within a composite mat is the moisture sorption model. Several are available in the literature (Malmquist 1958; Nelson 1983; Wu 1999; Dai and Yu 2004; Vidal Bastías and Cloutier 2005). Because of their complexity and nonlinearity, it is quite difficult to predict the impact of the sorption model used on the solution. The initial MC ( $M_{init}$ ) of the fiber mat is also expected to have an influence on the hygrothermal conditions within the mat during the hot pressing process. Thus, a closer look at those two important components should also be taken.

The objective of this work was to quantify the impact of variations of the fiber mat heat and mass transfer properties, initial MC, and moisture sorption model on the numerical solution of the heat and mass transfer model in terms of temperature, gas pressure, and MC. To achieve this objective, we performed a sensitivity study of the mathematical model to the mat physical properties and assumed boundary conditions. In this way, we account for the variability and uncertainty of the material properties and estimate their impact on the precision of the numerically predicted results. The most influential parameters will thus be identified. By presenting a deeper and broader insight into the influence of some of the material properties on the evolution of the internal environment of the fiber mat during the hot pressing process, this work can be seen as complementary to that of Zombori et al (2004).

## MATERIAL AND METHODS

### Material

Refined softwood MDF fibers were obtained from the Uniboard MDF La-Baie plant in Ville

de La-Baie, Quebec, Canada. The fibers were a blend of about 90% black spruce (*Picea mariana*) and 10% balsam fir (*Abies balsamea*). The fibers at 6.5% initial MC were blended with 12% (fiber oven-dry weight basis) urea-formaldehyde resin and 1% wax in a laboratory rotary drum blender. The initial MC of the furnish was 12%. A series of six MDF panels of size 560 × 460 × 13 mm and target density of 750 kg/m<sup>3</sup> at 8% MC were produced in a Dieffenbacher laboratory batch press equipped with a PressMAN measurement and control system. The press platens were at 203°C. The pressing schedule of 335 s was divided into five steps. The initial mat thickness of about 182 mm was reduced to 140% of the final thickness in the first 35 s (Step 1). The press remained in this position for the next 15 s (Step 2) followed by the second compression lasting 110 s at the end of which the mat reached its final thickness of 13 mm (Step 3). The hot platens remained in this position for the next 110 s (Step 4). The final step (Step 5) was the degassing period (65 s) during which the press was slowly opened and reached 107% of the final panel thickness at 335 s.

## Methods

**Overall approach and assumptions.** It was reported by Humphrey and Bolton (1989b) that the size of the board has an effect on the temperature and gas pressure within the hot pressed mat. In the current study, a single panel geometry was considered. Therefore, the effect of panel size was not studied. All the mats were formed using the same raw materials and hot pressed using the same pressing schedule.

Bound water was assumed to be in equilibrium with water vapor in the lumens and in the mat voids. Local thermodynamic equilibrium was assumed at every point of the fiber mat and the relationship among local MC, RH, and temperature was described by the sorption isotherms considered in this study. Hence, the three state variables of the model are temperature, air pressure, and vapor pressure. For the numerical study by the finite element method, the physical

model used is that proposed by Thömen and Humphrey (2006), and all of the material properties of the fiber mat were taken from the available literature. None of the fiber mat material properties was obtained from the panels produced in the laboratory.

The current study is focused on the heat and moisture transfer phenomena involved in the hot pressing of the MDF wood fiber mat. The rheology of mat consolidation was not explicitly considered in this study. Therefore, a pre-defined time- and space-dependent oven-dry vertical density profile based on the work of Wang and Winistorfer (2000) (see Appendix 1) was used in the simulations to update the local heat and moisture transfer properties and porosity of the mat. Consequently, the complex dynamic interactions between heat and moisture and rheological parameters involved during hot pressing process were not taken into account. We are aware that this simplification may have an influence on the model results presented in the current study. A numerical coupling between the mechanical and the heat and mass transfer models will be presented in future work. The results presented here should therefore be seen from the perspective of the numerical methods used and regarded as a numerical study by the finite element method of the sensitivity of a numerical heat and mass transfer model to some of the key mat properties and model parameters.

In the present work, we focused on the impact of thermal conductivity, gas permeability, and convective heat and mass transfer coefficients associated to the boundary conditions on the solution. Moreover, we examined the impact of the sorption model and the initial MC of the fiber mat on the results. It is assumed that the initial mat MC is uniform throughout the thickness. The contribution of resin cure to heat and mass transfer is not taken into account. All the results were obtained by finite element numerical simulations.

**Model of heat and mass transfer in the fiber mat.** We retained the mathematical model proposed by Thömen and Humphrey (2006). The

model is based on the mass conservation of air and water vapor and conservation of energy. We restate the original version of this model as follows in terms of the three state variables: partial air pressure ( $P_a$ ), partial water vapor pressure ( $P_v$ ), and temperature ( $T$ ):

Mass conservation of air

$$\begin{aligned} \frac{\partial(\rho_a \Phi)}{\partial t} - \nabla \cdot \left( \left[ \frac{\rho_a}{\mu} K_p + \frac{M_a}{RT} D_{eff} \right] \cdot \nabla P_a \right) \\ - \nabla \cdot \left( \frac{\rho_a}{\mu} K_p \cdot \nabla P_v \right) = 0 \end{aligned} \quad (1)$$

Mass conservation of water vapor

$$\begin{aligned} \frac{\partial(\rho_v \Phi)}{\partial t} - \nabla \cdot \left( \frac{\rho_v}{\mu} K_p \cdot \nabla P_a \right) \\ - \nabla \cdot \left( \left[ \frac{\rho_v}{\mu} K_p + \frac{M_v}{RT} D_{eff} \right] \cdot \nabla P_v \right) \\ = -\rho_{OD} \frac{\partial M}{\partial t} \end{aligned} \quad (2)$$

Energy conservation

$$\begin{aligned} \rho_{Mat} C_{Mat} \frac{\partial T}{\partial t} - H_{fg} \rho_{OD} \frac{\partial M}{\partial t} \\ - \nabla \cdot (K_T \cdot \nabla T) = 0 \end{aligned} \quad (3)$$

(see “Nomenclature” and Appendices 1 and 2 for definitions of variables and expressions). Using the Malmquist’s sorption model (Malmquist 1958; Vidal Bastías and Cloutier 2005), we can also predict and monitor the evolution of the mat MC with time at any position. As the MC  $M$  depends on temperature ( $T$ ) and partial vapor pressure ( $P_v$ ), the chain rule is applied and the term  $\frac{\partial M}{\partial t}$  is developed as  $\frac{\partial M}{\partial t} = \frac{\partial M}{\partial P_v} \frac{\partial P_v}{\partial t} + \frac{\partial M}{\partial T} \frac{\partial T}{\partial t}$ . This expression is then substituted into Eqs 2 and 3. The model is thus expressed in terms of the three state variables:  $P_a$ ,  $P_v$ , and  $T$ .

**Finite element solution strategy.** For each of the three conservation equations (Eqs 1, 2, and 3), a finite element method discretization is performed in space and the time derivatives are calculated using the Euler implicit scheme. Each state variable is discretized by Q1 (linear quadrangular) finite element.

Taking advantage of the symmetry, our computational domain represents a quarter of the full 2D geometry (see Fig 1). Therefore, for the numerical simulation runs, we consider a rectangular domain in the  $x$ - $z$  plane of the following dimensions: 280 mm (half length)  $\times$  6.5 mm (half thickness). Figure 1 shows details of the 2D geometry and our working domain. The domain considered for calculation was meshed with a  $16 \times 16$  grid having 256 rectangular elements.

The nonlinear Eqs 1, 2, and 3 are strongly coupled and form a coherent system, which can be written in the following general form:

$$\begin{aligned} \begin{bmatrix} a_{11} & 0 & a_{13} \\ 0 & a_{22} & a_{23} \\ 0 & a_{32} & a_{33} \end{bmatrix} \cdot \begin{bmatrix} \frac{\partial P_a}{\partial t} \\ \frac{\partial P_v}{\partial t} \\ \frac{\partial T}{\partial t} \end{bmatrix} \\ - \nabla \cdot \left( \begin{bmatrix} B_1 & B_2 & 0 \\ C_1 & C_2 & 0 \\ 0 & 0 & K \end{bmatrix} \cdot \begin{bmatrix} \nabla P_a \\ \nabla P_v \\ \nabla T \end{bmatrix} \right) = \begin{bmatrix} F_a \\ F_v \\ F_T \end{bmatrix} \end{aligned} \quad (4)$$

An integrated approach simultaneously considering all important variables during hot pressing was proposed by Kavvouras (1977), Humphrey (1982), and Bolton and Humphrey (1988). In the case of a heat and mass transfer model, we achieved it in the following way. At each time step and for each nonlinear iteration, the three equations forming this system are solved simultaneously preserving the full coupling between them. At each time step, the nonlinear system (Eqs 1, 2, and 3) is solved by a fixed point method allowing to predict the evolution of the state variables in space. During each time

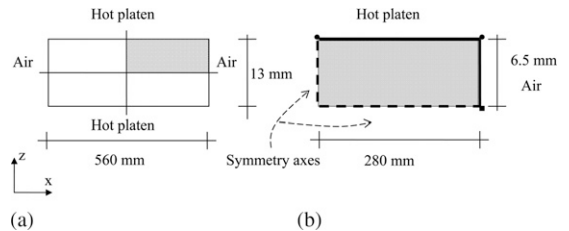


Figure 1. (a) Full 2D geometry of a fiber mat; (b) computational domain in 2D (one-quarter of the full geometry).

step, several iterations of a fixed point method are performed to reach convergence to  $10^{-6}$  in the residual norm. From one nonlinear iteration to another, all the local conditions and mat material properties are updated. This is somewhat different from the approach adopted by Thömen and Humphrey (2006). Indeed, these authors kept the local conditions and properties constant during a given time step (Thömen 2000). In our case, we updated values of all parameters for each nonlinear iteration within each time step.

Given that we use Euler implicit time scheme combined with the finite element method, we have no constraint on the time step length. However, a too large time step could cause convergence and precision problems. The results presented in this paper were obtained using a 0.1-s time step.

**Boundary conditions.** Appropriate boundary conditions are needed to properly solve Eqs 1, 2, and 3. The temperature evolution of the surface in contact with the hot platen (Fig 1a) was imposed by a Dirichlet boundary condition based on the data obtained during in situ laboratory experiments. The surface in contact with the hot platen includes the two end vertices illustrated by black dots in Fig 1b. Moreover, the following fluxes are considered at the boundaries:

$$\text{Heat flux : } q_T = -K_T \cdot \nabla T \quad (5)$$

$$\begin{aligned} \text{Air flux : } q_{Pa} = & - \left( \frac{\rho_a}{\mu} K_p \cdot \nabla P \right) \\ & - \left( \frac{M_a}{RT} D_{eff} \cdot \nabla P_a \right) \end{aligned} \quad (6)$$

$$\begin{aligned} \text{Vapor flux : } q_{Pv} = & - \left( \frac{\rho_v}{\mu} K_p \cdot \nabla P \right) \\ & - \left( \frac{M_v}{RT} D_{eff} \cdot \nabla P_v \right) \end{aligned} \quad (7)$$

The hot platen is assumed impervious to gas and therefore  $q_{Pa} = 0$  and  $q_{Pv} = 0$ . Symmetry conditions are imposed ( $q_T = 0$ ,  $q_{Pa} = 0$ ,  $q_{Pv} = 0$ ) on the two symmetry axis illustrated by dashed lines in Fig 1b. On the external edge in contact with the ambient air, the following convection

boundary conditions are imposed for the three state variables: temperature, air pressure, and vapor pressure, respectively:

$$q_T \cdot \vec{n} = -h_T \cdot (T - T_{amb}) \quad (8)$$

$$\begin{aligned} q_{Pa} \cdot \vec{n} = & -h_p \cdot \frac{\rho_a}{\mu} \cdot (P - P_{amb}) \\ & - 10^{-5} \cdot \frac{\rho_a}{P_a} \cdot (P_a - P_{a,amb}) \end{aligned} \quad (9)$$

$$\begin{aligned} q_{Pv} \cdot \vec{n} = & -h_p \cdot \frac{\rho_v}{\mu} \cdot (P - P_{amb}) \\ & - 10^{-5} \cdot \frac{\rho_v}{P_v} \cdot (P_v - P_{v,amb}) \end{aligned} \quad (10)$$

where  $\vec{n}$  is the outward unit normal vector, and  $h_T$  and  $h_p$  are, respectively, the convective heat and mass transfer coefficients at the edge. In Fig 1, the external edge is the right-hand side edge of the rectangular domain and is represented by a continuous black line including the black square (Fig 1b). The main mode of mass transfer between the mat and the environment is the gas bulk flow (Zombori et al 2004) generated by the difference of total gas pressure within and outside the mat. Diffusion generated by the difference of partial pressures within and outside the mat plays a secondary role (Zombori et al 2004).

**Sensitivity study.** The state variables ( $P_a$ ,  $P_v$ ,  $T$ ) of the heat and mass transfer model depend on many parameters describing the physical properties of the mat. In our sensitivity study, we perform “what if” scenarios with regard to variations in the material properties. The intuitive and simple approach adopted consists of perturbing one parameter, whereas all the others remain at their reference value. Therefore, the influence of one parameter at a time on the solution is examined.

The results obtained using reference values of the material properties proposed in the literature are compared with results obtained with perturbed values of the material properties. To some extent, the perturbation factors can be seen as uncertainty or measurement errors on the material property of interest. Hence, a perturbed value of a material

property of interest is obtained by multiplying the reference expression by a given factor. In this work, the results are presented for the following multiplying factors: 0.5, 0.8, and 0.9 for a decrease of 50, 20, and 10%, respectively; and 1.1, 1.2, and 1.5 for an increase of 10, 20, and 50%, respectively. Note that the perturbation coefficients are chosen within a reasonable range given that the variability of the material parameters and the uncertainty of the experimental measurements are quite large. Moreover, in their sensitivity study, Zombori et al (2004) considered constant reference values for parameters of interest. Furthermore, they presented a sensitivity study based on a single perturbation factor: 50% increase in the parameter reference value.

**Comparison of results.** The solution obtained with the perturbed value of a parameter is compared with that obtained using the reference value of the same parameter. The resulting discrepancy between those solutions can be quantified in different ways. We express it as a percentage of the maximum relative difference (MaxRelDiff). Therefore, we will monitor the evolution in time of the maximum relative deviation from the reference solutions. For instance,  $T_{\text{ref}}$  refers to the temperature field calculated using the reference values and  $T_{\text{per}}$  is the temperature calculated using a perturbed value of a parameter of interest. Therefore, at each time step, the following variable is calculated:

$$\text{MaxRelDiff} = 100 \cdot \text{sign}(T_{\text{per}} - T_{\text{ref}}) \cdot \max_{\Omega} \left| \frac{T_{\text{per}} - T_{\text{ref}}}{T_{\text{ref}}} \right| \quad (11)$$

where MaxRelDiff is the maximum relative difference in percentage depicting the impact of the variation of a given parameter on the temperature field. After each time step, the expression  $\left| \frac{T_{\text{per}} - T_{\text{ref}}}{T_{\text{ref}}} \right|$  is calculated over the simulation domain  $\Omega$  and its maximum value retained. It represents the largest relative discrepancy between the two solutions. However, it gives no indication on the location of the maximum deviation. The expression  $(T_{\text{per}} - T_{\text{ref}})$  is evaluated at the point corresponding to the largest relative dis-

crepancy between the two solutions and its sign is taken. The sign of the expression  $(T_{\text{per}} - T_{\text{ref}})$  indicates if the perturbed value of a parameter caused an increase in temperature (when the sign is positive) or a decrease (when the sign is negative). This generic approach is systematically used to quantify discrepancies for other variables of interest as well.

**Sorption models.** Several sorption models of solid wood are proposed in the literature. We chose some of the most frequently used sorption models and performed numerical simulations to characterize the impact of the sorption model on the solution. The following sorption models were considered.

**Malmquist.** Vidal Bastías and Cloutier (2005) compared several sorption models and their study showed that the Malmquist's sorption model gives the best overall fit to experimental EMC data. Therefore, our reference is Malmquist's sorption model (Malmquist 1958; Vidal Bastías and Cloutier 2005) expressing dimensionless MC  $M$  as a function of absolute temperature  $T$  and dimensionless RH  $h$ :

$$M_{\text{Malmquist}} = \frac{MS}{1 + N \left( \frac{1}{h} - 1 \right)^{\frac{I}{3}}} \quad (12)$$

where  $MS$ ,  $N$ , and  $I$  are second-order polynomials of the absolute temperature,  $T$ , defined as follows (Vidal Bastías and Cloutier 2005):

$$MS = 0.40221 - 9.736 \cdot 10^{-5} \cdot T - 5.8964 \cdot 10^{-7} \cdot T^2 \quad (13)$$

$$N = -2.6939 + 0.018552 \cdot T - 2.1825 \cdot 10^{-6} \cdot T^2 \quad (14)$$

$$I = 2.2885 - 0.0016742 \cdot T + 2.0637 \cdot 10^{-6} \cdot T^2 \quad (15)$$

**Hailwood-Horrobin (HH2).** The Hailwood and Horrobin model (Vidal Bastías and Cloutier 2005) was also considered. We used the two

hydrates version of that model expressing dimensionless MC  $M$  as a function of absolute temperature  $T$  and dimensionless RH  $h$ :

$$M_{HH2} = \frac{18}{M_p} \times \left[ \frac{K \cdot h}{1 - K \cdot h} + \frac{K_1 \cdot K \cdot h + 2 \cdot K_1 \cdot K_2 \cdot K^2 \cdot h^2}{1 + K_1 \cdot K \cdot h + K_1 \cdot K_2 \cdot K^2 \cdot h^2} \right] \quad (16)$$

where the molar mass of water is 18 g/mol and  $M_p$  is the molar mass of a polymer forming a hydrate expressed in units of g/mol. Polynomial expressions for  $M_p$ ,  $K$ ,  $K_1$ , and  $K_2$  are given as functions of absolute temperature  $T$  (Vidal Bastías and Cloutier 2005):

$$K = 0.68405 + 4.7238 \cdot 10^{-4} \cdot T - 3.3289 \cdot 10^{-8} \cdot T^2 \quad (17)$$

$$K_1 = 19.641 - 0.0587818 \cdot T + 4.05 \cdot 10^{-5} \cdot T^2 \quad (18)$$

$$K_2 = 2.6172 + 1.6795 \cdot 10^{-3} \cdot T - 6.414 \cdot 10^{-6} \cdot T^2 \quad (19)$$

$$M_p = -330.03 + 2.3468 \cdot T + 2.8368 \cdot 10^{-4} \cdot T^2 \quad (20)$$

**García.** García (2002) proposed the following sorption model expressing dimensionless MC  $M$  as a function of absolute temperature  $T$  and dimensionless RH  $h$ :

$$M_{Garcia} = \alpha \left[ \left( \frac{B}{h} \right)^D - 1 \right]^{\frac{-1}{C}} \quad (21)$$

where  $B = 1.09603$ ,  $C = 2.36069$ ,  $D = 1.84447$ , and

$$\alpha = A_1 \exp \left\{ - \left( \frac{T + A_2}{A_3} \right)^{A_4} \right\} \quad (22)$$

with  $A_1 = 0.186575$ ,  $A_2 = 751.85$ ,  $A_3 = 1163.31$ , and  $A_4 = 12.7441$ .

**Nelson.** Nelson (1983) proposed a sorption model used later by Wu (1999) and by Dai and Yu (2004). Dimensionless MC  $M$  is expressed as a function of absolute temperature  $T$ , dimensionless RH  $h$  and two material-related parameters denoted by  $A$  and  $B$ :

$$M_{Nelson} = B \left[ 1 - \frac{1}{A} \ln \left( -2.38846 \times 10^{-4} \cdot \frac{R \cdot T}{M_v} \cdot \ln(h) \right) \right] \quad (23)$$

where  $M_v$  is the molar mass of water (0.018015 kg/mol) and  $R$  is the universal gas constant (8.3143 J/mol K). Wu (1999) fitted EMC–RH data for different wood-based products to Nelson's sorption model to estimate the two material related parameters,  $A$  [dimensionless] and  $B$  [dimensionless]. For MDF, Wu (1999) found that during sorption,  $B = 0.1913$  and  $A = 4.68$ , whereas during desorption,  $B = 0.2494$  and  $A = 4.94$ . A difficulty arising in using Eq 23 is the appropriate choice of parameters  $A$  and  $B$ . Indeed, during hot pressing, we can be in sorption at a given location within the mat and in desorption at another location. Therefore, based on values proposed by Wu (1999), we performed simulation runs with Nelson's model using mean values for  $B$  and  $A$ , hence, we used  $B = 0.22035$  and  $A = 4.81$ .

**Initial MC of the mat.** Because the initial MC of the fiber mat ( $M_{init}$ ) is expected to have an influence on the internal conditions of the mat, its impact on the results was studied. We have chosen several values for  $M_{init}$  to reflect conditions normally encountered in practice. Indeed, tests were made for the following dimensionless values of  $M_{init}$ : 0.08, 0.10, 0.12, and 0.14. We selected 0.12 as a reference value for the initial MC.

**Thermal conductivity of the mat ( $K_T$ ).** We used the expression suggested by Thömen and Humphrey (2006) as a reference value for the thermal conductivity of the fiber mat:  $K_{T_{xy}} = 1.5 \cdot K_{T_z}$  where

$$K_{T_z} = K_{T030} + \Delta K_T \quad (24)$$

$$K_{T030} = 4.38 \cdot 10^{-2} + 4.63 \cdot 10^{-5} \cdot \rho_{OD} + 4.86 \cdot 10^{-8} \cdot \rho_{OD}^2 \quad (25)$$

and

$$\Delta K_T = 0.49 \cdot M + (1.1 \cdot 10^{-4} + 4.3 \cdot 10^{-3} \cdot M) \cdot (T - 303.15) \quad (26)$$

The variables  $K_{Tz}$  and  $K_{Txy}$  represent, respectively, the thermal conductivity in the thickness and horizontal directions.  $K_{T030}$  is the thermal conductivity measured at 0%  $M$  and 30°C, and  $\Delta K_T$  is the correction term accounting for MC and temperature effects on thermal conductivity. The tensor of thermal conductivity  $K_T$  is therefore given in 2D by

$$K_T = \begin{bmatrix} K_{Txy} & 0 \\ 0 & K_{Tz} \end{bmatrix} \quad (27)$$

To characterize the impact of variations in thermal conductivity, simulations were performed with  $\alpha K_T$  where the perturbation factor  $\alpha$  took the values of 0.5, 0.8, 0.9, 1.1, 1.2, and 1.5.

#### **Specific gas permeability of the mat ( $K_p$ ).**

Analytical expressions for the specific gas permeability of MDF mats based on the curve fitting of experimental data can be found in García and Cloutier (2005) and also in von Haas et al (1998). The expression proposed by García and Cloutier (2005) is valid for MDF mats having a density of 400-1150 kg/m<sup>3</sup>, whereas in von Haas et al (1998), the permeability of fiber, particle, and strand mats with densities varying 200-1200 kg/m<sup>3</sup> was determined. The samples used by von Haas et al (1998) were prepared from consolidated panels with an adhesive content of 11%. In our study, the reference expression and the input data for the specific gas permeability of the MDF mats will be based on expressions proposed by von Haas et al (1998). Hence, the in-plane permeability ( $K_{pxy}$ ) and the cross-sectional permeability ( $K_{pz}$ ) of MDF fiber mats are both described by the following expression:

$$\exp\left(\frac{1}{A}\right) \quad (28)$$

where

$$A = a + b \cdot \rho_{Mat} + \frac{c}{\ln(\rho_{Mat})} \quad (29)$$

and the coefficients to determine  $K_{pxy}$  are  $a = -0.041$ ,  $b = 9.51 \cdot 10^{-6}$ ,  $c = -0.015$  and those for  $K_{pz}$  are  $a = -0.037$ ,  $b = 1.1 \cdot 10^{-5}$ ,  $c = -0.037$ .

The tensor  $K_p$  of the specific gas permeability of the MDF fiber mat is therefore given in 2D by

$$K_p = \begin{bmatrix} K_{pxy} & 0 \\ 0 & K_{pz} \end{bmatrix} \quad (30)$$

To examine the influence of variations in specific gas permeability, simulations were run with  $\alpha K_p$  where the perturbation factor  $\alpha$  took the values previously listed.

**Convective heat transfer coefficient on the external boundary ( $h_T$ ).** The sensitivity of the system's solution to variations of the convective heat transfer coefficient associated with the external boundary was also examined. The reference value for this parameter is  $h_T = 0.35$  and is taken from Zombori (2001) and Vidal Bastías (2006). When simulations are run with a perturbed value of  $h_T$ , the heat flux at the edge in contact with the surroundings becomes:

$$q_T \cdot \vec{n} = -\alpha \cdot h_T \cdot (T - T_{amb}) \quad (31)$$

where the perturbation factor  $\alpha$  is taking the same values as previously.

**Convective mass transfer coefficient on the external boundary ( $h_p$ ).** The convective mass transfer coefficient associated with the external boundary represents the fiber mat boundary gas transport properties and depicts the resistance to gas flow out of the mat. We examine the impact of this external bulk flow coefficient associated with the boundary condition imposed on the edge in contact with the ambient air. A reference value for this coefficient is  $h_p = 10^{-11}$ , which is somewhat different from that used by Zombori et al (2004) for flakeboards. Given that the contribution of diffusion to mass transport out of the mat is not significant (Zombori et al 2004), variations in  $h_p$  will affect the air and vapor fluxes

at the edge in contact with the surroundings. Therefore, the simulations were run with the following conditions at the external edge:

$$q_{Pa} \cdot \vec{n} = \alpha \cdot \left[ -h_p \cdot \frac{\rho_a}{\mu} \cdot (P - P_{amb}) - 10^{-5} \cdot \frac{\rho_a}{P_a} \cdot (P_a - P_{a,amb}) \right] \quad (32)$$

$$q_{Pv} \cdot \vec{n} = \alpha \cdot \left[ -h_p \cdot \frac{\rho_v}{\mu} \cdot (P - P_{amb}) - 10^{-5} \cdot \frac{\rho_v}{P_v} \cdot (P_v - P_{v,amb}) \right] \quad (33)$$

where a perturbation factor  $\alpha$  is taking the same values as previously.

## RESULTS AND DISCUSSION

Temperature and gas pressure were measured during the pressing process at the center of the panel plane at three points across mat thickness: the core, one-quarter of the thickness, and the surface. The temperature measurements are presented, together with numerically predicted results, in Fig 2a.<sup>1</sup> The total gas pressure curves are shown in Fig 2b. The model captures major trends and gives results of comparable quality to those of Zombori et al (2004) and Thömen and Humphrey (2006). It should be kept in mind that the numerical model used here is based solely on heat and mass transfer mechanisms and that the influence of the changing MC and temperature on rheological mechanisms was not considered. Moreover, the fiber mat material properties, including thermal conductivity, gas permeability, and porosity, were taken from the literature and not determined from the specific material used to make the panels in the laboratory. This can explain the discrepancies between the model and experimental results shown in Fig 2.

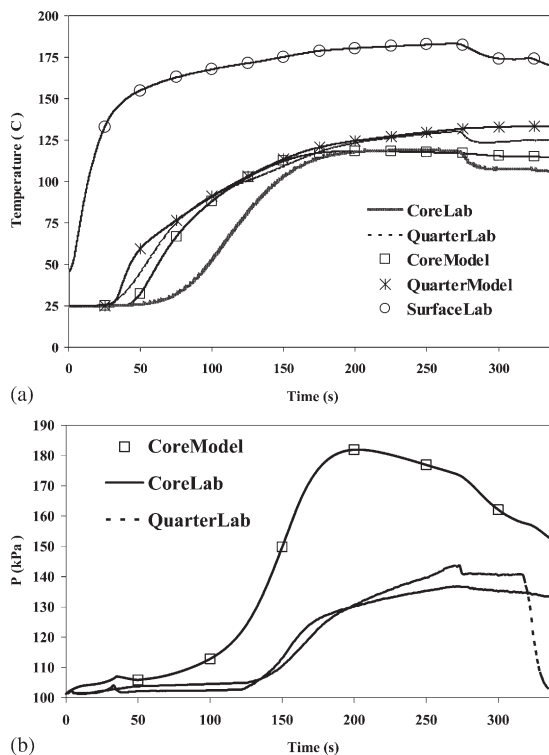


Figure 2. (a) Temperature evolution in time: measured and numerically predicted results. Curve labeled SurfaceLab is the temperature measured in laboratory at the surface in contact with the hot platen and was imposed as a Dirichlet boundary condition for T at the surface. On the other hand, curves labeled CoreModel and QuarterModel are obtained by numerical simulation and represent the temperature at the center and at one-quarter of the thickness, respectively. (b) Total gas pressure evolution in time: measured and numerical results. Curve labeled CoreModel is obtained by numerical simulation and the other two are measured in laboratory.

## Effect of Sorption Models

Figure 3 presents the comparison of the results for  $P$  at the core,  $M$  at the core, and  $M$  at one-quarter of the mat thickness obtained using each one of the four sorption models considered. Figure 4 shows the evolution in time of MaxRelDiff for  $T$ ,  $M$ , and  $P$ .

As can be seen in Fig 4, the Hailwood-Horrobin two-hydrate sorption model produces closer results to the reference sorption model (Malmquist). On the other hand, the Nelson (1983) model with

<sup>1</sup>In all figures, special symbols such as  $\square$ ,  $\circ$ ,  $*$ ,  $\diamond$ , etc. are used to distinguish different curves and do not represent experimental data unless the contrary is explicitly indicated.

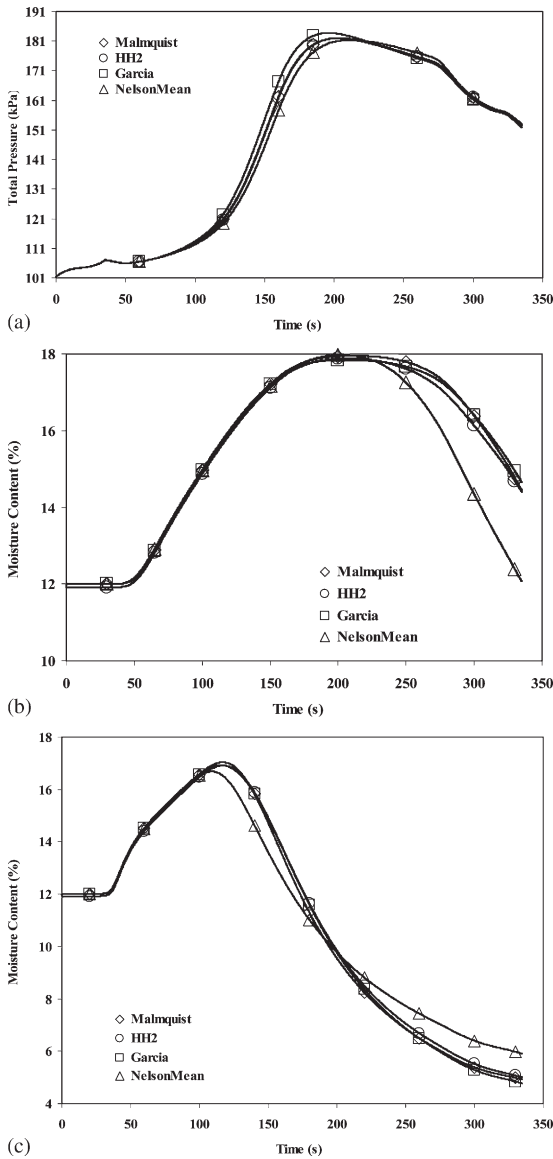


Figure 3. Solutions obtained with different sorption models for: (a) total gas pressure,  $P$ , at the core; (b) MC,  $M$ , at the core; (c) MC,  $M$ , at a quarter of the mat thickness. Note: In all figures presented in this document, special symbols like  $\square$ ,  $\circ$ ,  $*$ ,  $\diamond$ ,  $\Delta$  are used to distinguish different curves from each other and they do not represent experimental data unless the contrary is explicitly indicated.

averaged coefficients for MDF (Wu 1999) gives the results that are the most different from those obtained using Malmquist’s model. It should not be forgotten that the MaxRelDiff corresponds to

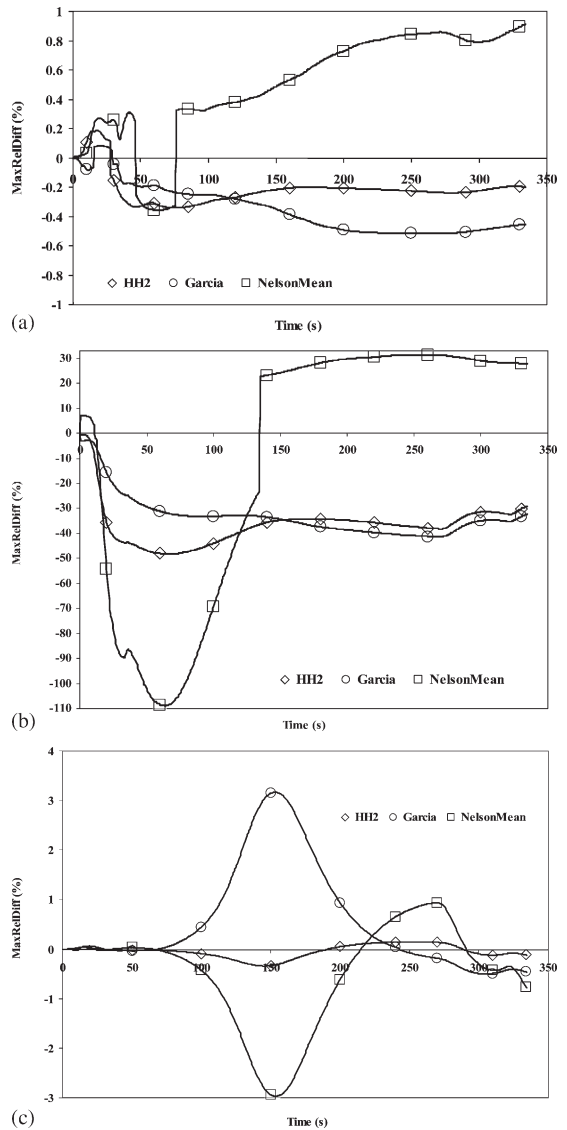


Figure 4. Effect of sorption models on: (a) temperature,  $T$ ; (b) MC,  $M$ ; (c) total gas pressure,  $P$ . Graphs present the maximum relative deviation of results obtained for each sorption model when compared with the reference solutions obtained with the Malmquist’s sorption model.

the largest discrepancy in the domain considered (Eq 11).

Temperature and internal gas pressure do not seem to be significantly influenced by the sorption model used (Figs 3 and 4). The effect of the sorption model on the MC evolution is more

significant. This was expected because different sorption models describe differently the EMC–RH– $T$  relationship.

### Effect of the Initial MC on the Predicted Results

Figure 5 summarizes the results obtained for  $P$  and  $M$  using each one of the four values of  $M_{init}$ . Figure 6 shows the evolution in time of the MaxRelDiff (Eq 11) for  $T$ ,  $M$ , and  $P$ . From Fig 6a, one could conclude that  $M_{init}$  does not seem to have a large impact on the evolution of temperature within the fiber mat. However, the evolution of MC within the mat is strongly dependent on  $M_{init}$  of the fiber mat (Fig 6b), which was expected and observed experimentally by Zombori et al (2004). Given that the evolution of the temperature field is very similar for different values of the initial MC considered, the amount of bound water desorbed should therefore be higher for higher values of  $M_{init}$ . Hence, the internal gas pressure consequently increases within the mat, as illustrated in Fig 5a. This is in agreement with observations made by Zombori et al (2004) claiming that the total pressure increases with increasing MC. Therefore, these results confirm that lowering the initial MC of the mat results in lower gas pressure within the mat during the hot pressing process.

### Effect of Thermal Conductivity ( $K_T$ )

Figure 7 presents the impact of variations in thermal conductivity ( $K_T$ ) on temperature, MC, and total pressure. When the thermal conductivity ( $K_T$ ) of the mat is decreased, heat is conducted more slowly through the mat and its internal temperature remains lower (Fig 7a). Hence, less bound water is desorbed resulting in a lower internal gas pressure. Of course, local MC will decrease more slowly as well. Conversely, if  $K_T$  is increased, heat is conducted more quickly through the mat and the local temperature increases (Fig 7a) causing the desorption of more bound water. This lowers local MC and more water vapor is produced, increasing internal gas pressure. As can be seen in Figs 7b and 7c,  $K_T$

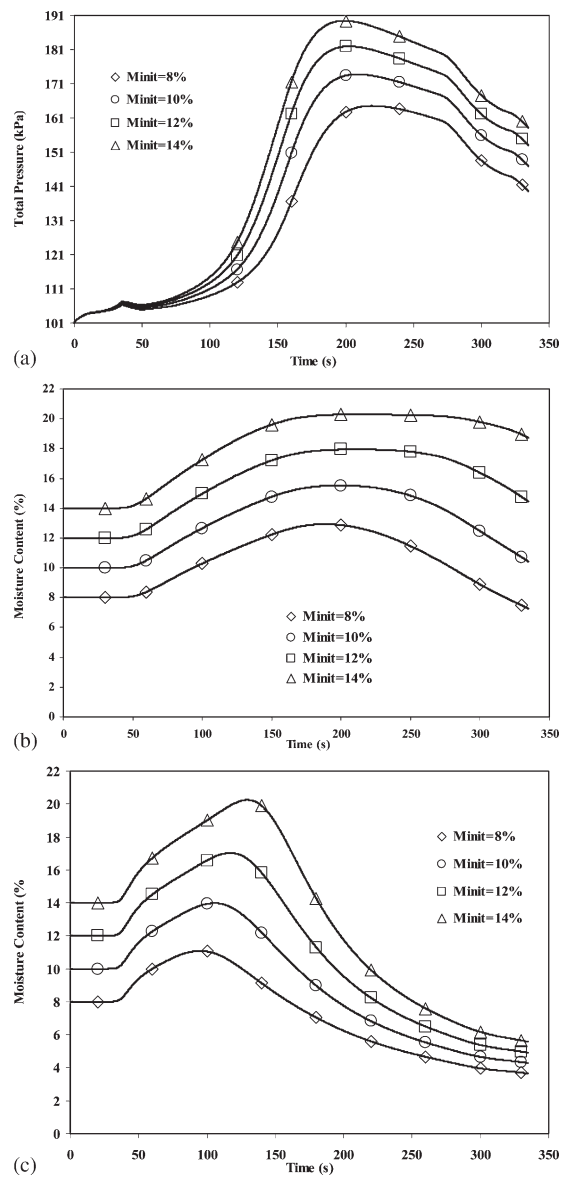


Figure 5. Solutions obtained with different values on initial MC,  $M_{init}$ , of the fiber mat for: (a) total gas pressure,  $P$ , at the core; (b) MC,  $M$ , at the core; (c) MC,  $M$ , at a quarter of the mat thickness.

has a very significant impact on mass transfer in the mat during the hot pressing process. Indeed, on average, variations in  $K_T$  have an effect on gas pressure in the mat almost five times greater than on temperature (Fig 7c). A similar effect can be observed on MC (Fig 7b). Moreover, variations

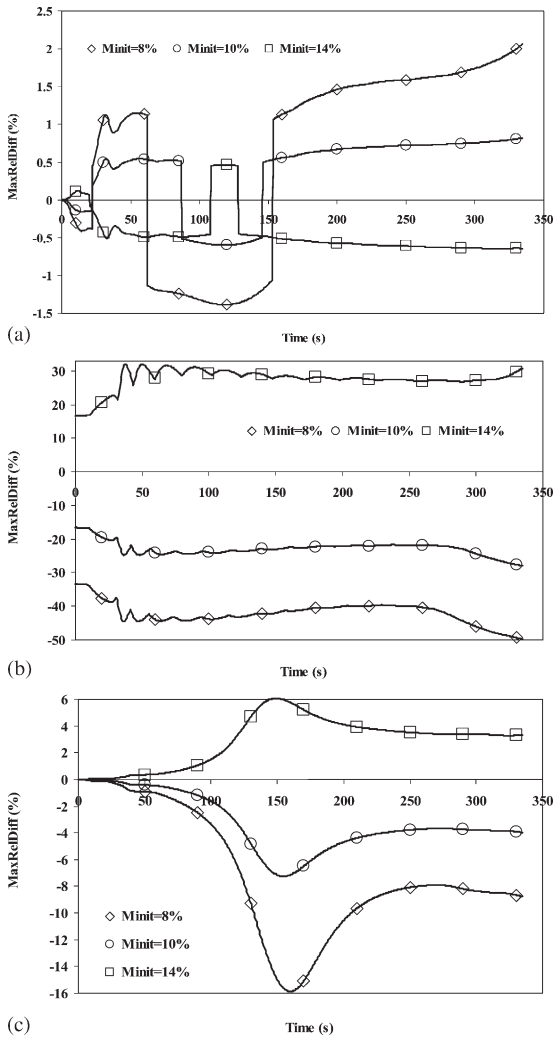


Figure 6. Effect of initial MC,  $M_{init}$ , of the mat on: (a) temperature,  $T$ ; (b) MC,  $M$ ; (c) total gas pressure,  $P$ . Graphs present the maximum relative deviation of results obtained for different values of  $M_{init}$  from the reference solutions obtained with  $M_{init} = 12\%$ .

in MC seem to be more or less linearly related to variations in thermal conductivity in the sense that, for instance, a perturbation of 10 or 20% in  $K_T$  of the mat will, respectively, induce a 10 or 20% variation in MC. Indeed, variations in thermal conductivity seem to affect mainly MC and total gas pressure. Zombori et al (2004) also concluded that variations in  $K_T$  have the most significant effect on the system.

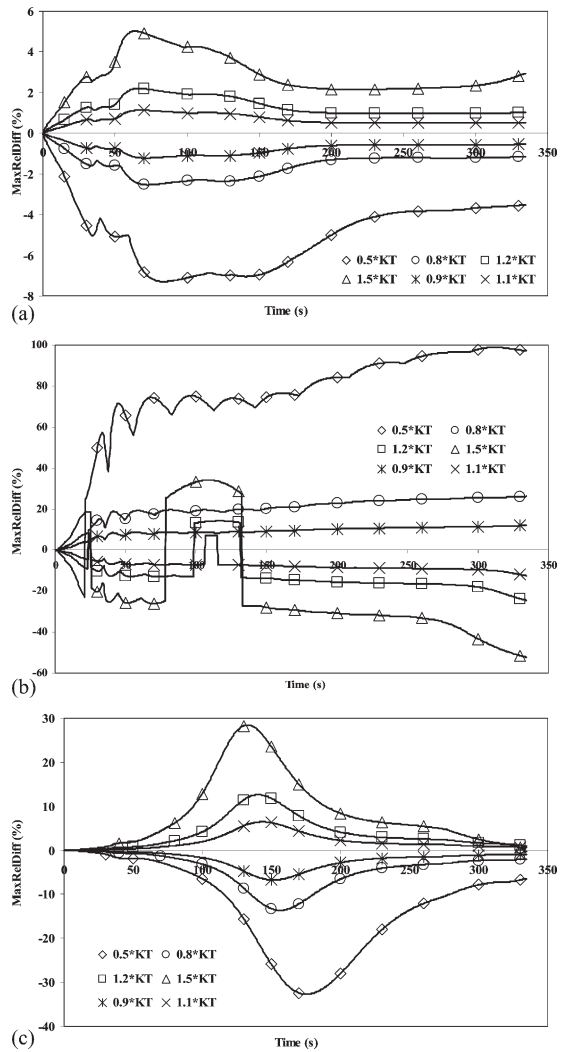


Figure 7. Effect of thermal conductivity  $K_T$  on: (a) temperature,  $T$ ; (b) MC,  $M$ ; (c) total gas pressure,  $P$ . Graphs present the maximum relative deviation of results obtained for different values of  $K_T$  from the reference solutions obtained with the reference value of  $K_T$ .

### Effect of the Specific Gas Permeability of the Mat ( $K_p$ )

Numerical simulations were run with perturbed values of  $K_p$ . The results are summarized in Fig 8 as a percentage of the maximum relative difference (Eq 11). As expected, Fig 8 suggests that gas permeability is a significant factor

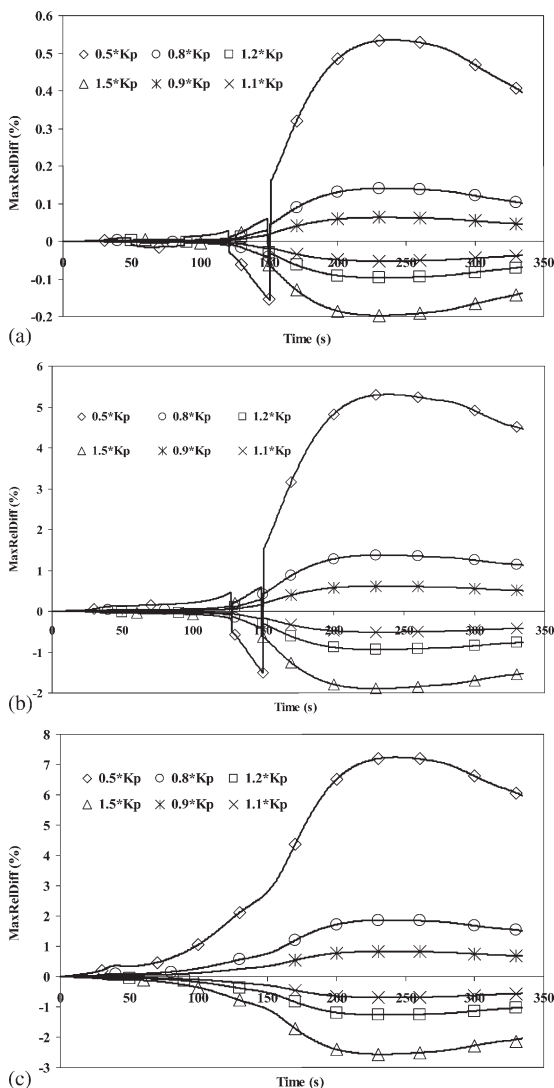


Figure 8. Influence of gas permeability  $K_p$  on: (a) temperature,  $T$ ; (b) MC,  $M$ ; (c) total gas pressure,  $P$ . Graphs present the maximum relative deviation of results obtained for different values of  $K_p$  from the reference solutions obtained with the reference value of  $K_p$ .

affecting mostly mass transfer within the mat. The sensitivity of the system to  $K_p$  and its influence on bulk flow within the mat was recognized by Zombori et al (2004). Indeed, MC and internal gas pressure seem to be about 10 times more sensitive than temperature to variations of  $K_p$ . It can also be noticed that a decrease in  $K_p$

appears to have a more pronounced effect on the solution than the proportional increase of  $K_p$ .

The higher the gas permeability, the easier the gas escapes the mat lowering total internal gas pressure. Thus, high gas permeability creates conditions that facilitate bound water desorption, which decreases mat MC. Bound water desorption and evaporation require a certain amount of energy (heat of sorption and latent heat of vaporization) that will cause a decrease in local temperature. On the other hand, when gas permeability decreases, the local gas pressure increases. This can result in water vapor condensation and an increase of the local MC. Water vapor condensation and adsorption are exothermic processes that release the latent heat of vaporization and the heat of sorption. This input of thermal energy increases the local temperature within the mat.

#### Effect of the Convective Heat Transfer Coefficient on the External Boundary ( $h_T$ )

Figure 9 depicts the sensitivity of the system's solution to variations of  $h_T$ . We concur with Zombori et al (2004) who found that  $h_T$  does not have a significant influence on heat and mass transfer phenomena within the mat. Indeed, the results presented in Fig 9 suggest that the convective energy transfer through the interface between the mat and the ambient air is not a significant factor.

#### Effect of the Convective Mass Transfer Coefficient on the External Boundary ( $h_p$ )

The convective mass transfer coefficient associated with the external boundary depicts the resistance to gas flow out of the mat. Figure 10 summarizes the impact of  $h_p$  on  $T$ ,  $M$ , and  $P$ . One observes that this coefficient has a very significant impact, especially on mass transfer within the mat. This is expressed by the significant impact of  $h_p$  on  $M$  and  $P$ . Indeed, these two variables seem to be 10 times more sensitive than temperature to variations of  $h_p$ . When the external mass transfer coefficient  $h_p$  decreases,

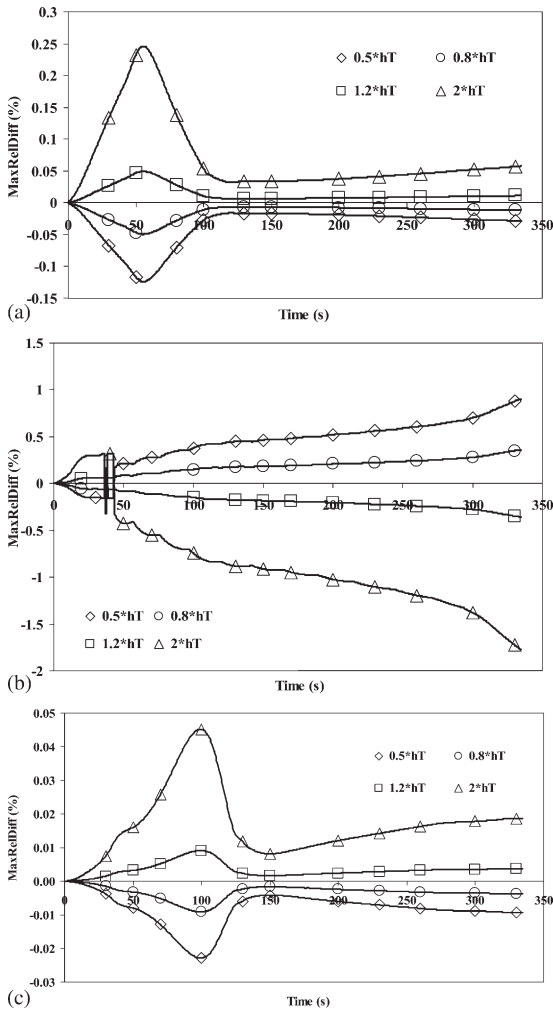


Figure 9. Influence of external heat transfer coefficient  $h_T$  on: (a) temperature, T; (b) MC, M; (c) total gas pressure, P. Graphs present the maximum relative deviation of results obtained for different values of  $h_T$  from the reference solutions obtained with the reference value  $h_T = 0.35$ .

the resistance to gas flow out of the mat increases. Hence, the gas remains trapped within the mat, increasing the internal gas pressure. Water vapor can condense, increasing mat MC. Water vapor condensation and adsorption in the wood fibers releases thermal energy (latent heat of vaporization and heat of sorption), slightly increasing the local temperature. If  $h_p$  increases, the opposite happens. The gas can leave the mat more easily, decreasing the internal gas pressure

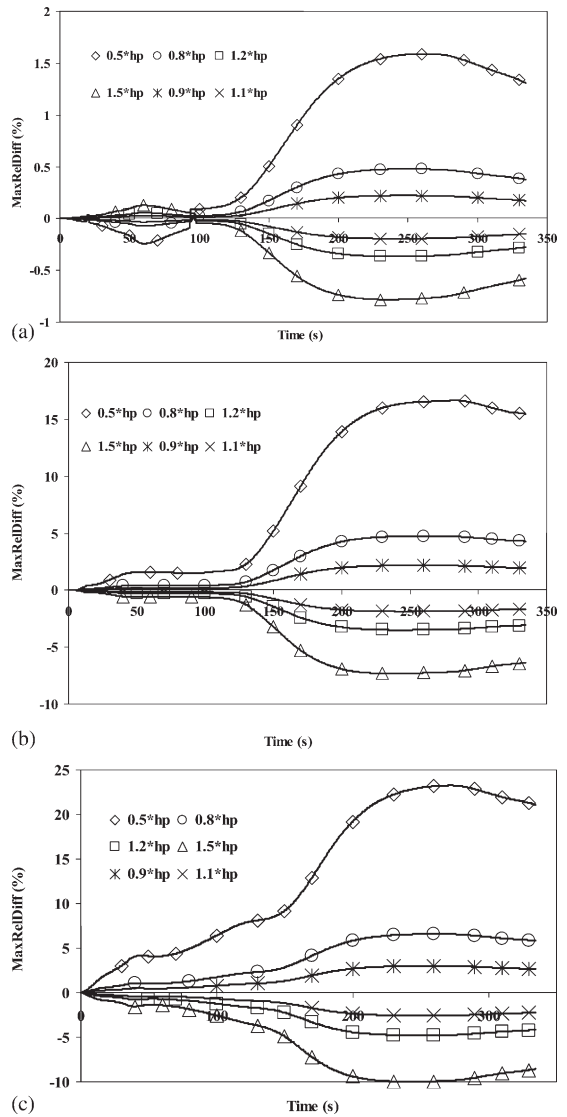


Figure 10. Influence of external convective mass transfer coefficient  $h_p$  on: (a) temperature, T; (b) MC, M; (c) total gas pressure, P. Graphs present the maximum relative deviation of results obtained for different values of  $h_p$  from the reference solutions obtained with the reference value of  $h_p = 10^{-11}$ .

and temperature. A lower gas pressure eases the bound water desorption process that eventually decreases local MC. The system seems to react more strongly to variations of  $h_p$  than to variations of  $K_p$ . Among the parameters we studied,  $h_p$  is the second most influential after  $K_T$ . It

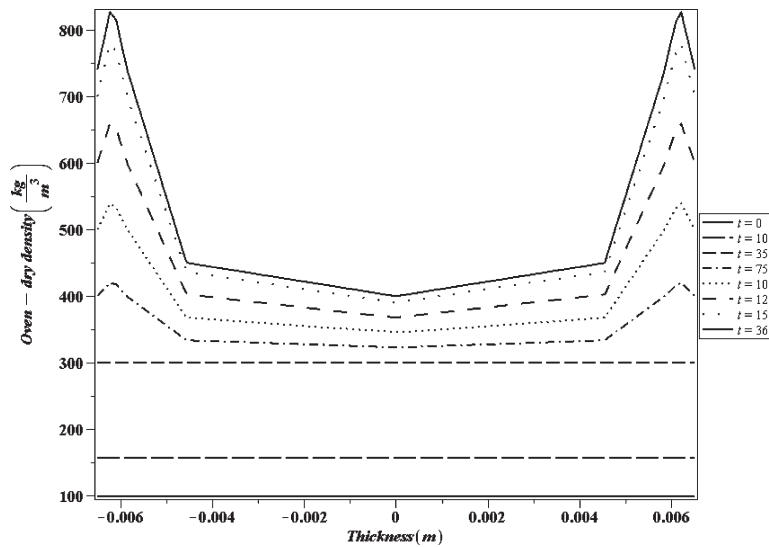


Figure 11. Evolution of a space and time dependent predefined oven-dry density profile used in calculations: density profile in thickness direction at different moments in time.

should be noticed that in their study on the influence of external bulk flow coefficient for flakeboard, Zombori et al (2004) concluded that this parameter does not noticeably influence the results. This difference may be explained by the higher porosity and gas permeability of MDF compared with flakeboard. It is therefore plausible that variations in  $h_p$  have a larger impact for MDF.

#### CONCLUSIONS

The coupled nature, complexity, and high nonlinearity of the equations constituting the model studied here make it difficult to predict the impact of uncertainties of the input variables on numerical solutions of the model. To gain insight of the influence of different parameters on the system's behavior, a sensitivity study of a numerical model of heat and mass transfer in the MDF mat during hot pressing was performed. Our study suggests that among the tested material properties, those having the most pronounced effect on heat and mass transfer within the mat during the hot pressing process are the thermal conductivity of the mat and the convective mass transfer coefficient associ-

ated with the edge in contact with the ambient air. Given that the latter coefficient plays a very important role in the quality of the results produced by the model, significant efforts should be made to get accurate measurements of this coefficient. Indeed, a variation of 20% of the reference value of  $h_p$  produces relative discrepancies up to 5% in MC and gas pressure results. The same variation of the reference value of gas permeability creates discrepancies in MC and total gas pressure that are lower than 2%. A variation of 50% of  $h_p$  leads to a relative difference of up to 15% in MC and up to 22% in gas pressure relative deviation. A similar perturbation of gas permeability induces variations in MC and gas pressure no greater than 5 and 7%, respectively. Given that the convective heat transfer coefficient does not seem to be an influential factor, accurate measurements of thermal conductivity, gas permeability, and convective mass transfer coefficient associated with the edge in contact with the ambient air are needed to improve the quality and reliability of model predictions. Also, the choice of an appropriate sorption model should be addressed with caution because of its impact on the numerically predicted values of MC. Finally,

lowering the initial MC of fiber mats contributes to lower internal gas pressure and helps achieve drier conditions within the mat.

#### NOMENCLATURE

- t: time [s]  
 x: length [m]  
 y: width [m]  
 z: thickness [m]  
 T: temperature field [K]; a state variable calculated by the model  
 $P_a$ : partial air pressure [Pa]; a state variable calculated by the model  
 $P_v$ : partial vapor pressure [Pa]; a state variable calculated by the model  
 P: total gas pressure [Pa]  
 M: moisture content [dimensionless]  
 h: relative humidity [dimensionless]  
 $P_{vSAT}$ : saturated vapor pressure [Pa]  
 $M_a$ : molar mass of air [kg/mol]  
 $M_v$ : molar mass of water vapor [kg/mol]  
 R: universal gas constant [J/(mol·K)]  
 $\rho_a$ : density of air [kg/m<sup>3</sup>]  
 $\rho_v$ : density of water vapor [kg/m<sup>3</sup>]  
 $\rho_{OD}$ : oven-dry density of the mat [kg/m<sup>3</sup>] (see Appendix 1)  
 $\Phi$ : porosity of the mat [dimensionless]  
 $\rho_{Mat}$ : wet density of the mat [kg/m<sup>3</sup>]  
 $K_T$ : thermal conductivity tensor [J/(m·s·K)]  
 $K_p$ : tensor of specific (effective) gas permeability of the mat [m<sup>3</sup>/m]  
 $D_{eff}$ : tensor of effective diffusion coefficient [m<sup>2</sup>/s]  
 $D_{va}$ : binary molecular diffusion coefficient of the air–vapor gas mixture [m<sup>2</sup>/s]  
 $k_d$ : obstruction factor [dimensionless]  
 $H_{fg}$ : latent heat of vaporization (desorption + evaporation) of bound water [J/kg]  
 $C_{Mat}$ : mass specific heat capacity of the mat at current moisture content [J/(kg·K)]  
 $\mu$ : dynamic viscosity of the air–vapor mixture [Pa·s]  
 $\mu_a$ : dynamic viscosity of the air [Pa·s]  
 $\mu_v$ : dynamic viscosity of the water vapor [Pa·s]  
 $h_T$ : convective heat transfer coefficient associated to the external boundary [J/(m<sup>2</sup>·s·K)]  
 $h_p$ : convective mass transfer coefficient associated to the external boundary [m]  
 $q_T$ : heat flux [J/(m<sup>2</sup>·s)]  
 $q_{Pa}$ : air flux [kg/(m<sup>2</sup>·s)]  
 $q_{Pv}$ : water vapor flux [kg/(m<sup>2</sup>·s)]  
 EMC: equilibrium moisture content  
 RH: relative humidity  
 $M_{init}$ : initial moisture content of the mat [dimensionless]  
 $T_{init}$ : initial temperature of the mat [K]  
 $h_{init}$ : initial value of relative humidity [dimensionless]  
 $P_{vSAT\ init}$ : initial value of saturated vapor pressure [Pa]  
 $P_{v\ init}$ : initial value of partial vapor pressure [Pa]  
 $P_{a\ init}$ : initial value of partial air pressure [Pa]  
 $T_{surface}$ : temperature at the surface in contact with the hot platen [K]  
 $h_{amb}$ : relative humidity of ambient gas [dimensionless]  
 $T_{amb}$ : temperature of the ambient gas [K]  
 $P_{vSAT\ amb}$ : saturated vapor pressure in ambient gas [Pa]  
 $P_{amb}$ : ambient gas pressure [Pa]  
 $P_{v\ amb}$ : ambient vapor pressure [Pa]  
 $P_{a\ amb}$ : ambient air pressure [Pa]

#### ACKNOWLEDGMENTS

The authors thank the Natural Sciences and Engineering Research Council of Canada (NSERC), FPInnovations–Forintek Division, Uniboard Canada, and Boa-Franc for funding of this project under the NSERC Strategic Grants program.

#### REFERENCES

- Bolton AJ, Humphrey PE (1988) The hot pressing of dry-formed wood-based composites. Part I. A review of the

- literature, identifying the primary physical process and the nature of their interaction. *Holzforshung* 42(6):403-406.
- Bolton AJ, Humphrey PE, Kavvouras PK (1989a) The hot pressing of dry-formed wood-based composites. Part III. Predicted pressure and temperature variation with time, and compared with experimental data for laboratory board. *Holzforshung* 43(4):265-274.
- Bolton AJ, Humphrey PE, Kavvouras PK (1989b) The hot pressing of dry-formed wood-based composites. Part IV. Predicted variation of mattress moisture content with time. *Holzforshung* 43(5):345-349.
- Bolton AJ, Humphrey PE, Kavvouras PK (1989c) The hot pressing of dry-formed wood-based composites. Part VI. The importance of stresses in the pressed mattress and their relevance to the minimisation of pressing time, and the variability of board properties. *Holzforshung* 43(6):406-410.
- Carvalho LM, Costa C (1998) Modeling and simulation of the hot-pressing process in the production of medium density fiberboard (MDF). *Chem Eng Commun* 170:1-21.
- Dai C, Yu C (2004) Heat and mass transfer in wood composite panels during hot-pressing: Part 1. A physical-mathematical model. *Wood Fiber Sci* 36(4):585-597.
- García P (2002) Three-dimensional heat and mass transfer during oriented strandboard hot-pressing. PhD thesis, University of British Columbia. 254 pp.
- García RA, Cloutier A (2005) Characterization of heat and mass transfer in the mat during the hot pressing of MDF panels. *Wood Fiber Sci* 37(1):23-41.
- Humphrey PE (1982) Physical aspects of wood particle-board manufacture. PhD thesis, University of Wales, Cardiff, Wales, UK.
- Humphrey PE, Bolton AJ (1989a) The hot pressing of dry-formed wood-based composites. Part II. A simulation model for heat and moisture transfer, and typical results. *Holzforshung* 43(3):199-206.
- Humphrey PE, Bolton AJ (1989b) The hot pressing of dry-formed wood-based composites. Part V. The effect of board size: Comparability of laboratory and industrial pressing. *Holzforshung* 43(6):401-405.
- Kavvouras PK (1977) Fundamental process variables in particleboard manufacture. PhD thesis, University of Wales, Cardiff, Wales, UK. 156 pp.
- Loxton C, Thumm A, Grigsby WJ, Adams TA, Ede RM (2003) Resin distribution in medium density fiberboard. Quantification of UF resin distribution on blow line and dry-blended MDF fiber and panels. *Wood Fiber Sci* 35(3):370-380.
- Malmquist L (1958) Sorption a deformation of space. Svenska Traforskningsinstitutet. *Trateknik. Meddelande*. 983, Stockholm, Sweden.
- Nelson RM Jr. (1983) A model for sorption of water by cellulosic materials. *Wood Fiber Sci* 15(1):8-22.
- Nigro N, Storti M (2006) Hot-pressing process modeling for medium density fiberboard (MDF). <http://arxiv.org/abs/math.NA/0010173> (August 11, 2008).
- Siau J (1984) Transport processes in wood. Springer-Verlag. 245 pp.
- Thömen H (2000) Modeling the physical process in natural fiber composites during batch and continuous pressing. PhD thesis, Oregon State University, Corvallis, OR. 187 pp.
- Thömen H, Humphrey PE (2006) Modeling the physical process relevant during hot pressing of wood-based composites. Part 1. Heat and mass transfer. *Holz Roh Werkst* 64:1-10.
- Vidal Bastías M (2006) Modélisation du pressage à chaud des panneaux de fibres de bois (MDF) par la méthode des éléments finis. PhD thesis, Université Laval, Québec, Canada. 158 pp.
- Vidal Bastías M, Cloutier A (2005) Evaluation of wood sorption models for high temperatures. *Maderas Cienc Tecnol* 7(2):145-158.
- von Haas G, Steffen A, Fruhwald A (1998) Untersuchungen zur permeabilität von faser-, span- und OSB-matten für gase. *Holz Roh Werkst* 56:386-392.
- Wang S, Winistorfer PM (2000) Fundamentals of vertical density profile formation in wood composites. Part 2. Methodology of vertical density formation under dynamic conditions. *Wood Fiber Sci* 32(2):220-238.
- Wu Q (1999) Application of Nelson's sorption isotherm to wood composites and overlays. *Wood Fiber Sci* 31(2):187-191.
- Zombori BG (2001) Modeling the transient effects during the hot-pressing of wood-based composites. PhD thesis, Virginia Tech, Blacksburg, VA. 212 pp.
- Zombori BG, Kamke FA, Watson LT (2003) Simulation of the internal conditions during the hot-pressing process. *Wood Fiber Sci* 35(1):2-23.
- Zombori BG, Kamke FA, Watson LT (2004) Sensitivity analysis of internal mat environment during hot pressing. *Wood Fiber Sci* 36(2):195-209.

## APPENDIX 1

A predefined mat oven-dry vertical density profile ( $\rho_{OD}$  [kg/m<sup>3</sup>]) was used for calculations. This profile is space and time dependent and is based on the results presented by Wang and Winistorfer (2000). The mathematic representation of the density profile is given by the expression presented subsequently. For the sake of clarity, this expression is graphically presented in Fig 11 to illustrate the density profile as a function of time and space (position in the thickness direction). Because the symmetry of the vertical density profile is assumed, its evolution is only presented for half of the mat thickness. In the mathematical expression of the profile, "t" represents time and "z" represents position in the thickness direction. Furthermore, in the thickness ("z") direction, the

density profile is divided into four sections. In each section, the density profile is expressed by a different function. Of course, the overall continuity of the density profile is ensured by the way the four functions are constructed. These functions are defined as follows:

*LD* = Low-Density Section,

*MD* = Medium-Density Section,

*HD1* = First Part of the High-Density Section,

*HD2* = Second Part of the High-Density Section.

$$\rho_{OD} = \left\{ \begin{array}{ll} LD & 0 \leq |z| \leq 0.00455 \\ MD & 0.00455 < |z| < 0.00585 \\ HD1 & 0.00585 \leq |z| \leq 0.006175 \\ HD2 & 0.006175 < |z| \leq 0.0065 \end{array} \right\}$$

where

$$LD = \left\{ \begin{array}{ll} 5.736968 \cdot t + 99.206112 & 0 \leq t \leq 35 \\ 300 & 35 < t \leq 50 \\ 300 + (t - 50) \cdot (0.909091 + 99.9001 \cdot |z|) & 50 < t \leq 160 \\ 400.00001 + 10989.011 \cdot |z| & 160 < t \end{array} \right\}$$

$$MD = \left\{ TPLD + (|z| - 0.00455) \cdot \frac{(BPHD - TPLD)}{(0.00585 - 0.00455)} \quad 0 \leq t \right\}$$

$$TPLD = \left\{ \begin{array}{ll} 5.736968 \cdot t + 99.206112 & 0 \leq t \leq 35 \\ 300 & 35 < t \leq 50 \\ 231.8181772 + 1.363636455 \cdot t & 50 < t \leq 160 \\ 450.00001 & 160 < t \end{array} \right\}$$

$$BPHD = \left\{ \begin{array}{ll} 5.736968 \cdot t + 99.206112 & 0 \leq t \leq 35 \\ 300 & 35 < t \leq 50 \\ 100 + 4 \cdot t & 50 < t \leq 160 \\ 740 & 160 < t \end{array} \right\}$$

$$HD1 = \left\{ \begin{array}{ll} 5.736968 \cdot t + 99.206112 & 0 \leq t \leq 35 \\ 300 & 35 < t \leq 50 \\ 300 + (t - 50) \cdot (-12.36363636 + 2797.202797 \cdot |z|) & 50 < t \leq 160 \\ -1060 + 3.076923077 \cdot 10^5 \cdot |z| & 160 < t \end{array} \right\}$$

$$HD2 = \left\{ \begin{array}{ll} 5.736968 \cdot t + 99.206112 & 0 \leq t \leq 35 \\ 300 & 35 < t \leq 50 \\ 300 + (t - 50) \cdot (22.18181827 - 2797.202797 \cdot |z|) & 50 < t \leq 160 \\ 2740.00001 - 3.076923077 \cdot 10^5 \cdot |z| & 160 < t \end{array} \right\}$$

## APPENDIX 2

Expressions of some parameters used in the calculations.

$P = P_a + P_v$ : Dalton's law

$M$ : defined at every point in the mat by a sorption model, we use Malmquist's sorption model as a reference

$$M_{Malmquist} = \frac{MS}{1 + N \left( \frac{1}{h} - 1 \right)^3}$$

where  $MS$ ,  $N$  and  $I$  are second order polynomials of absolute temperature  $T$  [K] given by

$$MS = 0.40221 - 9.736 \cdot 10^{-5} \cdot T - 5.8964 \cdot 10^{-7} \cdot T^2$$

$$N = -2.6939 + 0.018552 \cdot T - 2.1825 \cdot 10^{-6} \cdot T^2$$

$$I = 2.2885 - 0.0016742 \cdot T + 2.0637 \cdot 10^{-6} \cdot T^2$$

$$h = \frac{P_v}{P_{vSAT}}$$

$$P_{vSAT} = \exp \left\{ 53.421 - \frac{6516.3}{T} - 4.125 \cdot \ln(T) \right\}$$

(Kirchoff's formula)

$$M_a = 28.951 \cdot 10^{-3}$$

$$M_v = 18.015 \cdot 10^{-3}$$

$$R = 8.314147$$

$$\rho_a = \frac{M_a P_a}{RT} \text{ (ideal gas law)}$$

$$\rho_v = \frac{M_v P_v}{RT} \text{ (ideal gas law)}$$

$$\Phi = 1 - \frac{\rho_{OD}}{1530} \text{ (Siau 1984)}$$

$$\rho_{Mat} = \rho_{OD}(1 + M)$$

$$D_{eff} = \frac{D_{va}}{k_d} I, \text{ where } I \text{ is identity tensor}$$

$$D_{va} = 2.6 \cdot 10^{-5} \cdot \left( \frac{101325}{P} \right) \cdot \left( \frac{T}{298.2} \right)^{1.75}$$

$$k_d = 0.334 \cdot e^A, \quad A = 5.08 \cdot 10^{-3} \cdot \rho_{Mat}$$

$$H_{fg} = 2.511 \cdot 10^6 - 2.48 \cdot 10^3 \cdot (T - 273.15) + 1.172 \cdot 10^6 \cdot e^{-0.15 \cdot M \cdot 100}$$

$$C_{Mat} = \frac{1131 + 4.19 \cdot (T - 273.15) + 4190 \cdot M}{1 + M}$$

$$\mu = \frac{P_a}{P} \mu_a + \frac{P_v}{P} \mu_v$$

$$\mu_a = \frac{1.37 \cdot 10^{-6} \cdot T^{1.5}}{T + 85.75}$$

$$\mu_v = \frac{1.12 \cdot 10^{-5} \cdot T^{1.5}}{T + 2937.85}$$

$$h_T = 0.35$$

$$h_p = 10^{-11}$$

$$M_{init} = 0.12$$

$$T_{init} = 298.15$$

$h_{init}$  calculated by Malmquist's formula

$$\frac{1}{h_{init}} = 1 + \left[ \frac{1}{N_{init}} \left( \frac{MS_{init}}{M_{init}} - 1 \right) \right]^{\frac{3}{I_{init}}}$$

where

$$MS_{init} = 0.40221 - 9.736 \cdot 10^{-5} \cdot T_{init} - 5.8964 \cdot 10^{-7} \cdot T_{init}^2$$

$$N_{init} = -2.6939 + 0.018552 \cdot T_{init} - 2.1825 \cdot 10^{-6} \cdot T_{init}^2$$

$$I_{init} = 2.2885 - 0.0016742 \cdot T_{init} + 2.0637 \cdot 10^{-6} \cdot T_{init}^2$$

$$P_{vSAT init} =$$

$$\exp \left\{ 53.421 - \frac{6516.3}{T_{init}} - 4.125 \cdot \ln(T_{init}) \right\}$$

$$P_{vinit} = h_{init} \cdot P_{vSAT init}$$

$$P_{ainit} = 101325 - P_{vinit}$$

$T_{surface}$ : temperature at the surface in contact with the hot platen; its evolution in time is imposed by the Dirichlet boundary condition and the values are prescribed by measured experimental data (see Fig 1 and 2a)

$$h_{amb} = 0.3$$

$$T_{amb} = 298.15$$

$$P_{vSAT amb} =$$

$$\exp\left\{53.421 - \frac{6516.3}{T_{amb}} - 4.125 \cdot \ln(T_{amb})\right\}$$

$$P_{amb} = 101325$$

$$P_{v amb} = h_{amb} \cdot P_{vSAT amb}$$

$$P_{a amb} = P_{amb} - P_{v amb}$$